Distributions of ozone and some characteristics of the stratospheric aerosol reconstructed from data of space-based sensing of the Earth's twilight halo

S.V. Loginov and V.V. Butov

Institute of Optical Monitoring,
Siberian Branch of the Russian Academy of Sciences, Tomsk
Rocket & Space Corporation ENERGIYA, Korolev, Moscow Region

Received February 12, 2001

An iterative scheme and a technique of statistical regularization based on nonlinear programming were applied to optimize reconstruction of vertical profiles of the ozone concentration and aerosol extinction coefficient from data of space-based sensing of the Earth's twilight halo. These procedures enabled us to reduce the error of reconstruction down to 3% at a profile point and improved the profile resolution. As a result, the vertical structure of the reconstructed component can be obtained with a 100-m step. The procedures were applied to the experimental data obtained at Mir space station in 1989–1994.

Introduction

Studies of the atmosphere by methods of space-based remote sensing have been started in the early 1970s. In the pioneering paper,[1] the problem of determining characteristics of the field of stratospheric aerosol was solved using the method of sensing the twilight halo at large solar dip angles (>15°). Insufficient sensitivity of some devices, for example, Spektr-256 device makes it impossible using the approximation of the method of effective geometric shadow.[1] Devices mounted aboard such satellites as SBUV, LIMS, SAM, and SAGE have started the global monitoring of atmospheric components in the middle atmosphere. Advanced equipment was mounted on satellites of SAGE-II and NOAA types.[2,3] RSS-1 and RSS-2 devices having technical characteristics similar to that on SAGE-II were mounted on Soyuz-13 space craft and on the Salyut-1 space station.[4] The SAGE-II device that continued the series of experiments begun by SAM and SAGE had seven spectral channels in the visible and near-infrared spectral regions. A method was developed[2] for reconstruction of the vertical profile of ozone in the altitude range of 10–50 km accurate to 10%, and the profile of the aerosol extinction coefficient was reconstructed with the same accuracy in the altitude range of 10–20 km. The discretization step was 1 km. As a parameterization of the particle size-distribution function was used, some microphysical characteristics of aerosol were calculated.

Use of multichannel spectrometers such as Spektr-256, Gemma-2, and HIRS allows investigators (1) to obtain microphysical characteristics of aerosol without invoking parameterization of the particle size-distribution function and (2) to separate and calculate more accurately the concentrations of gaseous constituents that absorb radiation in the visible and near-infrared spectral regions. The Spektr-256 and Gemma-2 have about 500-m spatial resolution along the flight line, and the HIRS resolution is ~ 150 m. The altitude step is ~ 80 m. The use of multichannel spectrometers with the above characteristics increases the reliability and accuracy of studying the fine structure of distribution of atmospheric constituents.

1. Sensing of the Earth's twilight halo from space

The calculated results from Refs. 4 and 5 and our calculations suggest that when sensing the Earth's twilight halo from space (Fig. 1), starting from the ray altitude of 16 km, the device records radiation consisting mostly of the single-scattered solar radiation. As the ray altitude increases, the fraction of the single-scattered radiation in a ray increases roughly from 85% at the altitude of 16 km up to 97% at the altitude of 45 km. As applied to problems of twilight sensing, Kondratiev et al.[4] and Smoktii[5] concluded the following:

1. At small angles of the sun below the horizon, the curves of monochromatic brightness of twilight halo recorded with a space-borne spectrophotometer have a smooth structure without marked vertical depressions and gradients caused by local aerosol layers. Low value of brightness gradients caused by local aerosol layers at small angles of the sun below the horizon (< 3°) hampers solution of inverse problems of atmospheric optics.

2. Comparison of curves of monochromatic brightness of twilight halo calculated for different scattering phase functions has shown that the use of scattering phase functions calculated theoretically and determined from experimental data in the considered models of aerosol atmosphere (Elterman models of 1964, 1968 and Shifrin–Minin model) gives almost identical

0235-6880/01/08 639-07 $02.00

results at altitudes above 10–12 km. A marked difference is observed only in the lower 6-km atmospheric layer.

3. Reliable and stable manifestation of local aerosol layers as dark strips in the space images is possible only at large angles of the sun below the horizon (> 3°).

4. The presence of a reflecting surface at the atmospheric bottom level only slightly affects the spectral dependence of the halo brightness at all altitudes in the twilight zone. Calculations of the brightness of twilight halo by the Monte Carlo method for extreme values of the albedo (0 and 0.8) showed that at small angles of the sun below the horizon and small sighting azimuth the effect of the surface albedo on the Earth's brightness field in the twilight zone can be neglected at almost all altitudes. This conclusion is of particular significance for formulation and solution of inverse problems of atmospheric optics, because it allows neglecting, in sounding from space, the presence of a reflecting surface at the atmospheric bottom level.

5. From physical grounds it follows that, because of a small angular size of the twilight halo (2–3°) observed from an orbit, the degree of polarization of the halo radiation measured from space must be very low due to small value of the scattering angle of the direct solar radiation.

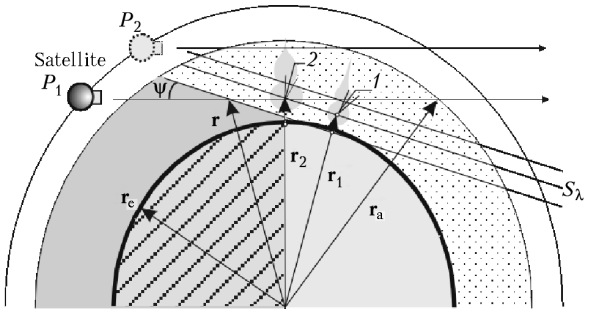

Fig. 1. Geometry of sensing the Earth's twilight halo from a space station.

It should be noted that local aerosol layers in the stratosphere were observed in experiments on twilight sensing of the Earth's halo from Mir station in 1992–1994. In three (of four) experiments, we have interpreted the sets of dark strips (four to seven strips) as local aerosol layers that are seen on the photos referencing the sighting line to the horizon. The thickness of the layers was equal, on the average, to 0.5 km and did not exceed 1 km. The distance between the layers was not constant, but varied from 2 to 5 km.

A significant point in solution of the inverse problem of sensing the twilight Earth's halo in order to find the vertical distribution of the aerosol field and the ozone concentration is the fact that in the approximation of small scattering angles the aerosol component determines the monochromatic brightness of the stratosphere and middle atmosphere in the visible and near-infrared spectral regions. This dependence becomes stronger if the stratosphere is polluted with aerosol, for example, after a volcanic eruption. In addition, the developed models of aerosol[6] assume only slight variability of the aerosol scattering phase function in the stratosphere and middle atmosphere. Therefore, we can reduce the requirement to the accuracy of setting the aerosol scattering phase function in inverse problems of remote sensing by use of the normalized monochromatic brightness provided that the condition

$$g_\lambda^{\mathrm{m}}(\psi)\ \beta_\lambda^{\mathrm{m}}(h) \ll g_\lambda^{\mathrm{a}}(h, \psi)\ \beta_\lambda^{\mathrm{a}}(h)$$

is fulfilled. Here $\beta_\lambda^{\mathrm{m}}(h)$ and $\beta_\lambda^{\mathrm{a}}(h)$ are the vertical profiles of the volume scattering coefficients of the molecular and aerosol components of the atmosphere, and $g_\lambda^{\mathrm{m}}(\psi)$ and $g_\lambda^{\mathrm{a}}(h, \psi)$ are the vertical profiles of the scattering phase functions of the molecular and aerosol atmospheric components, ψ is the scattering angle.

Thus, the use of sensing the twilight Earth's horizon from space and at small sun dip angles (< 3°) allows us, for altitudes above 25 km, to use single scattering approximation and neglect the surface albedo in calculations of monochromatic brightness. Therefore, we can write the following equation for the brightness of the twilight horizon:

$$I_\lambda(h, \psi) = I_{0\lambda}(h, \psi) + I_{1\lambda}(h, \psi), \qquad (1)$$

$$I_{0\lambda}(h, \psi) = B_\lambda(\psi), \quad I_{1\lambda}(h, \psi) = \int\limits_{r(h,\psi)}^{r_{\mathrm{a}}} [g_\lambda^{\mathrm{m}}(\psi)\ \beta_\lambda^{\mathrm{m}}(x) +$$

$$+ g_\lambda^{\mathrm{a}}(x, \psi)\ \beta_\lambda^{\mathrm{a}}(x)]\ \mathrm{e}^{-T_{2\lambda}(x,h,\psi)}\ B_\lambda(h, x, \psi)\ \mathrm{d}l(x, h).$$

In Eq. (1)

$$B_\lambda(h, x, \psi) = \int\limits_{r(h,x,\psi)}^{r_{\mathrm{a}}} S_\lambda(x, \psi)\ \mathrm{e}^{-T_{1\lambda}(x,h,\psi)}\ \mathrm{d}l(x, h);$$

$$B_\lambda(\psi) = 2 \int\limits_{r(\psi)}^{r_{\mathrm{a}}} S_\lambda(\psi)\ \mathrm{e}^{-T_\lambda(h,\psi)}\ \mathrm{d}l(h);$$

$$S_\lambda(\psi) = \pi D S_\lambda^0 \int K_\lambda^S(y, z)\ K(y, z, \psi)\ \mathrm{d}y\ \mathrm{d}z,$$

where $B_\lambda(h, x, \psi)$ is the brightness of a path element, $B_\lambda(h, \psi)$ is the source brightness attenuated by the atmosphere, $S_\lambda(h, \psi)$ is the brightness of an extended extraterrestrial source, S_λ^0 is the brightness at the center of the sun disk, D is the area of the sun disk not distorted by refraction, $K_\lambda^{\mathrm{S}}(y, z)$ is the brightness of an element on the sun disk (in relative units) depending on the distance y to the center, $K_\lambda^{\mathrm{d}}(y, h, \psi + \varepsilon)$ is the area of the disk element (in relative units) depending on the distance to the disk center and the degree to which the disk is deformed by atmospheric refraction $\varepsilon(h)$, $T_{1\lambda}(x, h, \psi)$ and $T_{2\lambda}(x, h, \psi)$ are the values of the optical thickness in the parts *1* and *2*, respectively (Fig. 1).

The recorded signal depends on both the scattered and "direct" solar radiation attenuated by the atmosphere. For this reason, we can separate out three situations:

1) the signal is formed by the twilight halo brightness

$$I_{1\lambda} \gg I_{0\lambda},\ I_\lambda(h, \psi) \cong U_\lambda(\psi) \int\limits_{r(h,\psi)}^{r_a} [g_\lambda^m(\psi)\ \beta_\lambda^m(x) +$$

$$+ g_\lambda^a(x, \psi)\ \beta_\lambda^a(x)]\ e^{-T_{2\lambda}(x,h,\psi)}\ B_\lambda(h, x, \psi)\ dl(x, h), \quad (2)$$

where $U_\lambda(\psi)$ is the transmittance of a window with the allowance made for both light absorption and scattering;

2) the signal is formed by scattering of direct solar radiation within the window

$$I_{1\lambda} << I_{0\lambda},\ I_\lambda(h, \psi) = I_{0\lambda}(h, \psi)\ U_\lambda(\psi), \quad (3)$$

3) the signal is distorted by a parasitic signal due to scattering of direct solar radiation within the window

$$I_{1\lambda} \approx I_{0\lambda},$$

$$I_\lambda(h, \psi) = I_{0\lambda}(h, \psi)\ U_\lambda(\psi) + I_{1\lambda}(h, \psi)\ U_\lambda(0).$$

By data filtering, the problem can be reduced to the first case.

Using normalization, we can reduce the right-hand side of Eqs. (2) and (3) to dimensionless parameters and the coefficient $U_\lambda(\psi)$ can be rejected. Therefore, the effect of window on the recorded signal is omitted in the following consideration.

Rewriting Eq. (2) in a matrix form, we obtain the matrix analog of the integral equation of the first kind, which can be solved by the method of successive approximations.[7]

The optical thickness $T_{2\lambda}(x, h, \psi)$ is a convex function. The source function $B_\lambda(h, x, \psi)$ is a combination of linear and convex operators; therefore, nonlinearity of Eq. (2) can be overcome by variational methods. The structure of the solving algorithm for the aerosol scattering cross section can be constructed as follows:

$$\int\limits_{r(h,\psi)}^{r_a} [g_\lambda^m(\psi)\ \beta_\lambda^m(x) + g_\lambda^a(x, \psi)\ \beta_\lambda^a(x)^{(p)}] \times$$

$$\times\ e^{-T_{2\lambda}(x,h,\psi)^{(p-1)}}\ B_\lambda(h, x, \psi)^{(p-1)}\ dl(x, h) \cong I_\lambda(h, \psi). \quad (4)$$

The stable solution of the ill-posed problem (4) is sought based on regularization methods.

The conditions for convergence of the iterative process (4) are the following:

(a) for aerosol

$$\Delta\boldsymbol{\beta} = [(\mathbf{A}\mathbf{A}^+ + \alpha\boldsymbol{\Omega})^{-1}\ \mathbf{A}^+]'_\beta\ \mathbf{A}\boldsymbol{\beta}\ \delta\boldsymbol{\beta},$$

$$\| \mathbf{V} \| = \| [(\mathbf{A}\mathbf{A}^+ + \alpha\boldsymbol{\Omega})^{-1}\ \mathbf{A}^+]'_\beta\ \mathbf{A}\boldsymbol{\beta} \| < 1,$$

$$\| \mathbf{V} \| = \| [(\mathbf{A}\mathbf{A}^+ + \alpha\boldsymbol{\Omega})^{-1}\ \mathbf{A}^+]'_\beta\ \mathbf{A}\boldsymbol{\beta} \| \le$$

$$\le \| (\mathbf{A}\mathbf{A}^+ + \alpha\boldsymbol{\Omega})^{-1} \| \| (\mathbf{A}^+)'_\beta\ \mathbf{A}^+ \| \| \boldsymbol{\beta} \| < 1,$$

where

$$a_{ij} = e^{-T_{2\lambda ij}}\ B_{\lambda\ ij}\ \Delta l_{ij},$$

$$\frac{\partial a_{ij}}{\partial \beta_{\lambda j}} = e^{-T_{2\lambda ij}}\ B_{\lambda\ ij}\ \Delta l_{ij} \left(- \frac{\partial (T_{2_\lambda})_{ij}}{\partial \beta_{\lambda j}} + \frac{\partial (\ln B_\lambda)_{ij}}{\partial \beta_{\lambda j}} \right);$$

(b) for ozone

$$\Delta\mathbf{F}_\lambda = (F_\lambda)'_\beta\ \Delta\boldsymbol{\beta} = \mathbf{A}\ \Delta\boldsymbol{\beta},$$

$$\Delta\boldsymbol{\beta} = (\mathbf{A}\mathbf{A}^+ + \alpha\boldsymbol{\Omega})^{-1}\ \mathbf{A}^+\ \Delta\mathbf{F}_\lambda\ \delta\boldsymbol{\beta} = (\mathbf{A}\mathbf{A}^+ + \alpha\boldsymbol{\Omega})^{-1}\mathbf{A}^+\ \mathbf{A}\ \Delta\boldsymbol{\beta}\ \delta\boldsymbol{\beta},$$

$$\mathbf{V} = (\mathbf{A}\mathbf{A}^+ + \alpha\boldsymbol{\Omega})^{-1}\ \mathbf{A}^+\ \Delta\mathbf{F}_\lambda = (\mathbf{A}\mathbf{A}^+ + \alpha\boldsymbol{\Omega})^{-1}\ \mathbf{A}^+\ \mathbf{A}\ \Delta\boldsymbol{\beta},$$

$$\| \mathbf{V} \| = \| (\mathbf{A}\mathbf{A}^+ + \alpha\boldsymbol{\Omega})^{-1}\ \mathbf{A}^+\ \mathbf{A}\Delta\boldsymbol{\beta} \| \le$$

$$\le \| (\mathbf{A}\mathbf{A}^+ + \alpha\boldsymbol{\Omega})^{-1} \| \| \mathbf{A}^+\ \mathbf{A} \| \| \Delta\boldsymbol{\beta} \| < 1.$$

Use of a multichannel spectrometer allows microphysical characteristics of the aerosol to be assessed from the data on scattering. For processing, we used the spectral regions 0.45–0.53 and 0.75–0.83 μm (the spectrometer operating range is 0.44–0.83 μm). The characteristics sought are the aerosol particle size-distribution function $f(R, h)$, R_f, and the refractive index m. They were determined from the condition

$$\| \beta_\lambda^a(h) - \beta_\lambda^a(h)_m \| = \min_{f,m,R_f}, \quad (5)$$

where

$$\beta_\lambda^a(h) = N(h) \int\limits_{R_0}^{R_f} \pi R^2\ Q(R, \lambda, m)\ f(R, h)\ dR,$$

$Q(R, \lambda, m)$ is the extinction efficiency factor calculated by the Mie theory for homogeneous spherical particles of radius R with the complex refractive index $m < 2$ (Ref. 8). Microphysical parameters of aerosol, such as the effective mean size of particles $<R>_{eff}$ and $<R^3>_{eff}$, were calculated as the mean values of the distributions $Rf(R, h)$ and $R^3 f(R, h)$ normalized to the number of aerosol particles having the size from $R_0 = 0.01$ to $R_f < 0.9$ μm. The errors of calculation were ~ 25–40% for $f(R)$, $<R>$, δR .

2. Results

2.1. Model studies

Reconstruction of aerosol scattering coefficient

Solution of the inverse problem involves the normalized signal. Due to normalization, the right-hand side of Eq. (4) reduces to dimensionless parameters, and the problem of reconstruction of the scattering coefficient is solved efficiently (with the discrepancy of 10%). This allows the results to be obtained even in the case that the optical characteristics of the window are unknown or outdated. To solve Eq. (4) for the extinction coefficient, we used iterative procedures[9]

based on the Martine–Kryanev algorithm and the technique of statistical regularization in combination with the scheme of nonlinear programming. As a result, the error of reconstruction, for the altitude range of 25–50 km, was decreased down to 3–5% at a profile node and the vertical resolution was improved to 100 m. For description of the procedures, see Appendix.

Reconstruction of the ozone concentration

In the problem of reconstruction of the ozone concentration, the signal is also reduced to a dimensionless parameter $F_\lambda = -\ln(I_\lambda / I_\lambda^{\mathrm{W}})$, where I_λ^{W} is the signal, in which absorption by the ozone is ignored, or $F_\lambda^* = -\ln(I_\lambda / I_\lambda^{\mathrm{W}} \| I_\lambda^{\mathrm{W}} \| / \| I_\lambda \|)$, where $\| I_\lambda \|$ and $\| I_\lambda^{\mathrm{W}} \|$ are norms of the signals with and without the regard for absorption by ozone, respectively,

$$I_\lambda^{\mathrm{W}} = I_{\lambda 1} (I_{\lambda 2} / I_{\lambda 1})^{\kappa},$$

where $\kappa = (\lambda - \lambda_1)/(\lambda_2 - \lambda_1)$, $\lambda_1 = 0.5$ μm, $\lambda_2 = 0.79$ μm.

Two techniques were used to determine the vertical profile of the ozone absorption coefficient.

1) A sort of the DIAL method. According to Ref. 10, let us use the formula $I_\lambda \approx I_\lambda^{\mathrm{W}} \, \mathrm{e}^{-T_\lambda^{\mathrm{oz}}}$, wherefrom $F_\lambda = T_\lambda^{\mathrm{oz}}$; T_λ^{oz} is the ozone optical depth along the parts *1* and *2* (see Fig. 1); it is related to the ozone absorption cross section by the integral equation

$$T_\lambda^{\mathrm{oz}} = \int_{r(h,\psi)}^{r_2} \beta_\lambda^{\mathrm{oz}}(x) \, \mathrm{d}l(x, h) + \int_{r_2}^{r} \beta_\lambda^{\mathrm{oz}}(x) \, \mathrm{d}l(x, h).$$

2) Newton method. Restricting our consideration to the series expansion of the functional F_λ or F_λ^* to the first order of smallness, we obtain

$$\Delta \mathbf{F}_\lambda = (F_\lambda)'_{\beta^{\mathrm{oz}}} \Delta \boldsymbol{\beta}^{\mathrm{oz}}, \quad \Delta \mathbf{F}_\lambda^* = (F_\lambda^*)'_{\beta^{\mathrm{oz}}} \Delta \boldsymbol{\beta}^{\mathrm{oz}},$$

or

$$\Delta \mathbf{F}_\lambda = (F_\lambda)'_\zeta \Delta \boldsymbol{\zeta}, \quad \Delta \mathbf{F}_\lambda^* = (F_\lambda^*)'_\zeta \Delta \boldsymbol{\zeta}, \quad \zeta(h) = \ln(\beta^{\mathrm{oz}}(h)).$$

The use of logarithmic derivative allows one to avoid negative values of the ozone concentration profile in the process of solution.

As the initial approximation, we used different variations of the model profile, including the profile consisting of constants. The algorithm converged in no more than 10 to 15 steps under the condition $\delta I < 10\%$. The discrepancy between the initial model profile of monochromatic brightness and the brightness profile obtained from the reconstructed profile of the scattering cross section was 5% with the variance of 5–10%. The same values were obtained with the use of the initial model brightness profiles calibrated to the profile norm or reference altitudes. The discrepancies for both F_λ and F_λ^* with respect to the initial model profile and the profile calculated from the reconstructed ozone absorption coefficient were 5–10%. The results of model studies and reconstructed results are shown in Fig. 2.

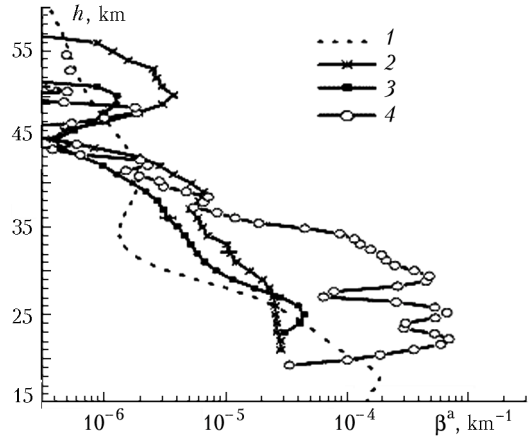

Fig. 2. Comparison of vertical profiles of aerosol extinction coefficient $\beta_\lambda^{\mathrm{a}}(h)$ at $\lambda = 0.828$ μm: model profile[14] (*1*); profile of 01.04.89 $B = -51.30°$, $L = 209.00°$ (*2*); profile of 03.07.89, $B = 51.20°$, $L = 188.00°$ (*3*); profile of 04.16.92, $B = 56.40°$, $L = 173.80°$ (*4*).

As the model experiments showed, application of twilight geometry of sensing allows the aerosol scattering cross section profiles and the ozone concentration profiles to be determined within the accuracy of 7 to 10% and discrepancy of 3–10% at the initial error of 5%.

2.2. Results of atmospheric sensing

The brightness of twilight Earth's horizon was measured with a spectrometer in 1989–1994 at different latitudes and in different seasons from Mir space station. The dates of observation and geographic coordinates of the device's sighting line are given in the Table.

Effective sizes of aerosol particles obtained in Atmosfera-2 (denominator) and SAGE-II (numerator[16]) experiments

Date	*B*	*L*	<*R*>, μm
01.04.89	– 51.3	209.0	/0.35
03.07.89	51.2	188.0	/0.40
04.16.92	56.4	173.8	0.53/0.57
04.05.94	46.0	177.1	0.33/0.34

Measurements were conducted during sunrise. At the moment of the device turn-on, the sighting line (SL) was at the altitude of 10–11 km, the angle of the sun below the horizon was 1.21–1.5°, and the azimuth angle was < 0.2°. Variations of sun elevation due to refraction were taken into account through the standard model of refraction.[11] The photographic reference allowed us to determine the distance between SL and the center of the sun disk, as well as to check ballistic calculations (accuracy of 1.5 km) using the degree of refraction deformation of the image of the sun disk. By the time the signal "went off scale," the range from 11 to 70 km had been scanned.

From processing the data of experiments by the scheme of sensing the twilight Earth's halo with a Spektr-256 multichannel spectrometer installed aboard Mir station, we have obtained the following results: (1) vertical

profiles of the ozone concentration and the aerosol extinction coefficient have been reconstructed with the error of 3–10% at a node and the discrepancy of 5–10% at the initial error of 5%; (2) the particle size-distribution functions were reconstructed with the error of 30–40% at the nodes for each altitude step. The results are shown in Figs. 2–4. The aerosol layer was observed in the altitude range of 50–55 km. The existence of this aerosol layer on the reconstructed profiles of the extinction coefficient corresponds to observations of the turbidity of the upper atmosphere at the Abastumanskaya Observatory by the method of twilight sensing[12] and the data of sensing from ASTRON astrophysical station.[13] In some measurements at the altitude of 49–50 km, aerosol was characterized by bimodal size distribution. The mean effective size of particles was 0.1–0.5 μm. For a comparison, Fig. 2 shows model profile from Ref. 14. A thick stratospheric aerosol layer at the altitude of 20–30 km (profile *4*, Fig. 2) was formed by an aerosol cloud that was produced at Mt. Pinatubo eruption (06.13.1991, $B = 15°$N, $L = 120°$E). The results obtained agree with the observations over the period since August 1991 until February 1992 (Refs. 15 and 16), in which the tendency to increase of the amount of aerosol in the stratosphere was noticed. Figure 3 shows the ozone profiles: profile reconstructed from data of sensing the twilight halo (*1*), profile plotted from the data of sensing with NOAA11 in nadir direction (the data borrowed from the serves ftp://toms.gsfc.nasa.gov/) (*2*), model profile plotted on data from Refs. 17 and 18 (*3*).

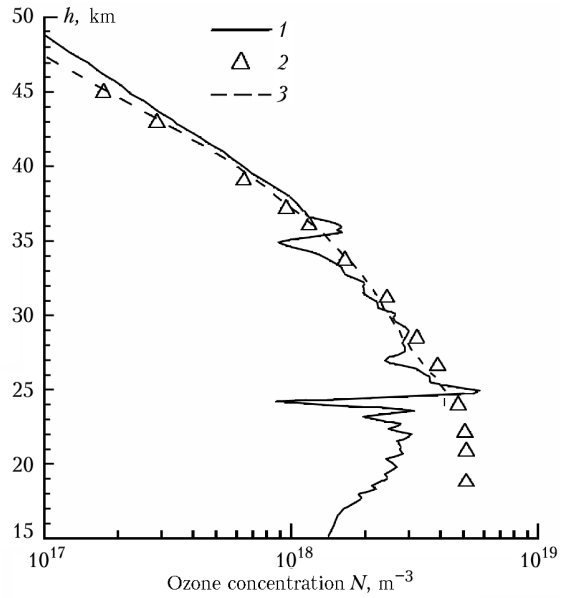

Fig. 3. Vertical profiles of the ozone: profile reconstructed from data of sensing the twilight halo (coordinates of under-perigee point $B = 56.40°$, $L = 173.8°$) (*1*), result of sensing with NOAA11 (coordinates of under-satellite point $B = 55.53°$, $L = 166.9°$) (*2*), and a model profile (*3*).

The difference between the ozone profiles for the altitudes < 25 km can be explained by the following facts. First, the single scattering approximation has different domains of applicability in describing the brightness of the twilight halo. The effects of multiple scattering manifest themselves at low altitudes starting from 25 km in the visible spectrum at scattering angles < 3°. This causes underestimation of the reconstructed profile of ozone concentration. The fraction of the multiple-scattered component makes up about 15% for the wavelength of 0.4 μm. Second, meridian coordinates of the points, for which the instantaneous concentration profiles were constructed in the Atmosfera-2 experiment and measured by NOAA11, differ by 7–10°. Third, at sensing along tangent paths in the tropopause and the lower stratosphere, the optical thickness in the visible spectrum and at the center of the Chappuis band increases markedly thus causing a decrease in the fraction of the valid signal.

The effective size of the stratospheric aerosol particles (determined from the results of the Atmosfera-2 experiment with the error about 30–40%) agrees with the estimates obtained in SAGE-II experiment. Table gives the values of mean "volume" radii of aerosol particles averaged over the vertical column from 20 to 50 km for every horizontal layer. These estimates were obtained from the experiments conducted using twilight sensing of the Earth's halo. Variation (in time) of the effective radii corresponding to the Northern Hemisphere is explained, first, by the decrease of volcanic emissions (Mt. Pinatubo) and, second, by the effect of meteor flows at the altitudes of 45–55 km. Our data differ from the data of Ref. 16 by 25%. This discrepancy does not exceed the error of determination of the size distribution function. It follows from analysis of Fig. 4 that aerosol layers characterized by large values of the mean effective radii and different values of the aerosol refractive index existed in the stratosphere ten months after Mt. Pinatubo eruption. The stability of estimation of the aerosol refractive index from the condition of minimum discrepancy of the extinction functional (5) was not studied. Therefore, the plot in Fig. 4*b* has only qualitative character.

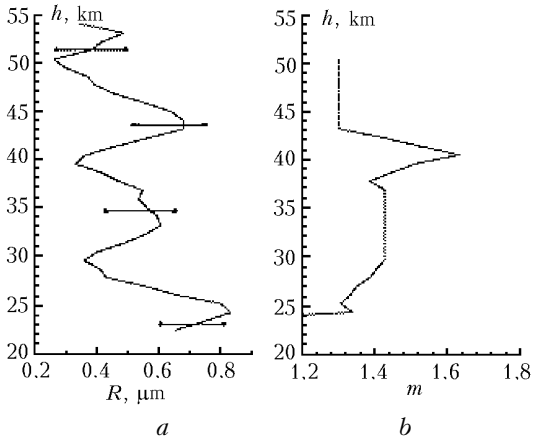

Fig. 4. Estimations of the mean volume radius <*R*> (*a*) and aerosol refractive index *m* (*b*). Measurements of 04.16.92.

Conclusion

The methods for solving the inverse problems of remote twilight sensing of the Earth's halo have been developed. The methods proposed were tested using data obtained in 1992–1994 from Mir space station.

Complex sensing of the middle atmosphere based on the use of the proposed methods of space sensing and ground-based instrumentation will provide for: (1) studying features in the spatial distribution of optically active atmospheric components, revealing stratification and microphysical characteristics of aerosol; (2) analyzing consequences of the complex effect of different factors on the formation of optical and microphysical properties of the aerosol and ozone components in the middle atmosphere, as well as the mutual effect of the components under study.

Acknowledgments

The authors are thankful to Prof. G.M. Grechko for the help in organization of the experiments.

APPENDIX

Regularization schemes

A. Regularization scheme based on nonlinear programming

To solve a problem of the type $\mathbf{K}\phi = \mathbf{f}$ for ϕ, an approach based on nonlinear programming can be used. This scheme has low sensitivity to the algorithm of selecting the stabilization parameter α and the structure of the stabilizer $\mathbf{\Omega}$ (Ref. 9). Consequently, calculation can be started from specifying the stabilizer and determination of α by any known method, for example, the iterative one:

$$\alpha^{(p)} = n/(\phi^{(p-1)}, \mathbf{\Omega}\phi^{(p-1)}).$$

here n is the dimension of ϕ.

Let us repeat reasoning from Ref. 9. The problem is reduced to determination of the conditional extremum

$$\min Z(\phi),\ \mathbf{H}\phi \geq \mathbf{h}, \qquad (A.1)$$

where $Z(\phi) = (1/2)(\phi, [\mathbf{K}^*\mathbf{W}\mathbf{K} + \alpha\mathbf{\Omega}]\phi) - (\mathbf{K}^*\mathbf{W}\mathbf{f}, \phi)$, $\mathbf{W}$ is the covariance matrix; the number of restrictive inequalities $\mathbf{H}\phi \geq \mathbf{h}$ is arbitrary.

Coming to the problem for unconditional extremum, let us write the Lagrange function in the form

$$L(\phi) = Z(\phi) + (\lambda, [\mathbf{h} - \mathbf{H}\phi]), \qquad (A.2)$$

and the vector of Lagrange factors $\lambda \geq 0$.

Find the saddle node $\{\phi_0, \lambda_0\}$ as a solution of the extremum problem (A.1). The vector ϕ_0 must be a stationary vector of the Lagrange function $L(\phi)$ at $\lambda = \lambda_0$:

$$\phi_0 = \mathbf{G}^{-1}(\mathbf{g} + \mathbf{H}^*\lambda_0), \qquad (A.3)$$

where

$$\mathbf{G} = \mathbf{K}^*\mathbf{W}\mathbf{K} + \alpha\mathbf{\Omega},\ \ \mathbf{g} = \mathbf{K}^*\ \mathbf{W}\mathbf{t}.$$

Substituting the general equation $\phi = \mathbf{G}^{-1}(\mathbf{g} + \mathbf{H}^*\lambda)$ in (A.2) and introducing the designations $\mathbf{V} = \mathbf{H}\mathbf{G}^{-1}\mathbf{H}$ and $\mathbf{v} = \mathbf{h} - \mathbf{H}\mathbf{G}^{-1}\mathbf{g}$, we obtain the following minimization problem:

$$\min_{\lambda>0} \{(1/2)\ (\lambda, \mathbf{V}\lambda) - (\lambda, \mathbf{v})\}, \qquad (A.4)$$

whose solution is λ_0. Substituting λ_0 in (A.3) we obtain the sought result.

The natural way to improve the solution is deformation of the grid with the subsequent revealing of a part, where ϕ_0 is monotonic or convex. For new parts, new inequalities $\mathbf{H}\phi \geq \mathbf{h}$ are written, and solution is repeated. Thus, the *a priori* information is successively complemented with the *a posteriori* one, and there is no need to correct α and $\mathbf{\Omega}$, because the significance of factors connected with the smoothness of the solution decreases. Systematic inclusion of new inequalities $\mathbf{H}\phi \geq \mathbf{h}$ in the algorithm should be made with care, since, for example, the use of conditions of monotonic or convex function may worsen the result and lead to manifestation of false structures.

B. Economical iterative algorithm with regularization

A convenient algorithm was proposed by Martine and Kryanev.[9] In the accepted designations it can be written as

$$(\mathbf{K}^*\mathbf{K} + \alpha\mathbf{\Omega})\phi^{(n)} = \alpha\mathbf{\Omega}\phi^{(n-1)} + \mathbf{K}^*\mathbf{f}. \qquad (A.5)$$

It was found that a less strict requirement could be imposed on selection of the regularization parameter in the Martine–Kryanev algorithm. It is necessary for the parameter not to be underestimated; overestimation of α as compared to its optimal value is not that significant — it manifests itself only in the increasing number of iterations. An acceptable condition for selection of α can be the equation:

$$\| \mathbf{K}^*\mathbf{K} \|_{L_2} \cong \alpha \| \mathbf{\Omega} \|_{L_2}.$$

Undoubted advantages of the algorithm (A.5) are its simplicity, high speed, high noise immunity, and possibility of flexibly varying the computational procedure due to variation of α and the number of measurements.

References

1. G.V. Rozenberg, Izv. Akad. Nauk SSSR, Ser. Fiz. Atmos. Okeana **1**, No. 2, 142–158 (1965).
2. P.-H. Wang and M.P. McCormick, J. Geophys. Res. D **94**, No. 6, 8435–8446 (1989).

3. J.M. Livingston and P.B. Russel, J. Geophys. Res. D **94**, No. 6, 8425–8433 (1989).
4. K.Ya. Kondratyev, G.I. Marchuk, A.A. Buznikov, et al., *Radiation Field of the Spherical Atmosphere* (Publishing House of the Leningrad State University, Leningrad, 1977), 216 pp.
5. O.I. Smoktii, *Modeling of Radiation Fields in Problems of Space Spectroscopy* (Nauka, Leningrad, 1986), 352 pp.
6. V.E. Zuev and G.M. Krekov, *Current Problems of Atmospheric Optics. Optical Models of the Atmosphere* (Gidrometeoizdat, Leningrad, 1986), Vol. 2, 256 pp.
7. I.E. Naats, *Method of Inverse Problem in Atmospheric Optics* (Nauka, Novosibirsk, 1986), 200 pp.
8. V.E. Zuev, *Propagation of Visible and Infrared Waves in the Atmosphere* (Sov. Radio, Moscow, 1970), 495 pp.
9. N.G. Preobrazhenskii and V.V. Pikalov, *Instable Problems of Plasma Diagnostics* (Nauka, Novosibirsk, 1982), 237 pp.
10. F.E. Volz and R.M. Goody, J. Atmos. Sci. **19**, 385–408 (1962).
11. G.M. Grechko, A.S. Gurvich, et al., Tr. S.I. Vavilov State Optical Institute **71**, Issue 205 (1989), 221 pp.
12. G.V. Rozenberg, I.G. Mel'nikova, and T.G. Megrelishvili, Izv. Akad. Nauk SSSR, Ser. Fiz. Atmos. Okeana **18**, No. 4, 363–372 (1982).
13. A.A. Cheremisin, L.V. Granitskii, V.M. Myasnikov, and N.V. Vetchinkin, Atmos. Oceanic Opt. **11**, No. 10, 952–957 (1998).
14. G.E. Krekov and R.F. Rakhimov, *Lidar Model of the Atmosphere* (Nauka, Novosibirsk, 1982), 198 pp.
15. V.V. Zuev, V.E. Zuev, and V.N. Marichev, Atmos. Oceanic Opt. **6**, No. 10, 672–686 (1993).
16. Stratospheric Aerosol Optical Depths, http://www.giss.nasa.gov/data/strataer/.
17. G.M. Keating and D.F. Young, in: *Handbook for MAP* (University of Illinois, IL, 1985), Vol. 6, pp. 205–230.
18. J.J. Barnet and M. Corney, in: *Handbook for MAP* (University of Illinois, IL, 1985), Vol. 16, pp. 47–85.